JACS
JOURNAL OF THE AMERICAN CHEMICAL SOCIETY
Article
pubs.acs.org/JACS

Elucidating the Mechanism of Multiferroicity in $(NH_4)_3Cr(O_2)_4$ and Its Tailoring by Alkali Metal Substitution

Raghabendra Samantaray,[†] Ronald J. Clark,[†] Eun S. Choi,[‡] and Naresh S. Dalal*[,†,‡]

[†]Department of Chemistry and Biochemistry, Florida State University, Tallahassee, Florida 32306, United States
[‡]National High Magnetic Field Laboratory, Tallahassee, Florida 32312-4005, United States

Supporting Information

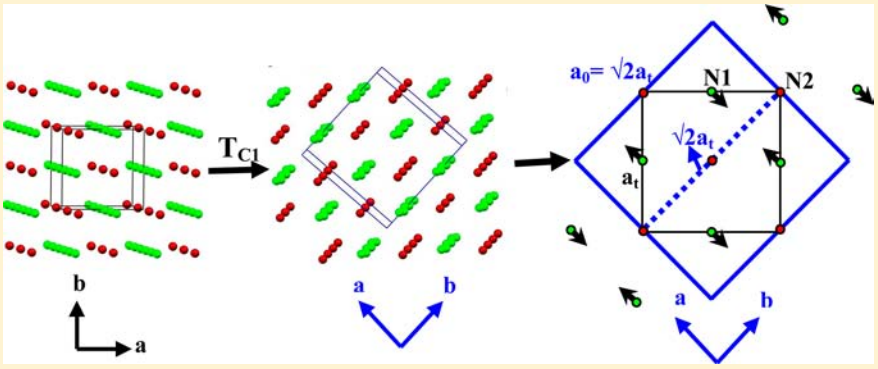

ABSTRACT: The antiferromagnetic Cr(V) peroxychromates, $M_3Cr(O_2)_4$, M = K, Rb, and Cs, become ferroelectric when mixed with NH_4^+, but the underlying mechanism is not understood. Our dielectric relaxation, Raman scattering, and high-frequency EPR measurements on the $M_{3-x}(NH_4)_xCr(O_2)_4$ family clarify this mechanism. At 295 K, $(NH_4)_3Cr(O_2)_4$ is tetragonal ($I\bar{4}2m$), with the NH_4^+ ions occupying two distinctly different sites, N1 and N2. A ferroelectric transition at T_{c1} = 250 K is revealed by λ-type anomalies in C_p and dielectric constant, and lowering of symmetry to C*mc*2(1). Below T_{c1}, the N1 sites lose their tetrahedral symmetry and thus polarization develops. Raman detection of translational modes involving the NH_4^+ ions around 193 cm^{-1} supports this model. EPR around T_{c1} revealed that the $[Cr(O_2)_4]^{3-}$ ions reorient by about 10°. A minor peak at $T_{c2} \approx 207$ K is attributed to a short-range ordering that culminates in a long-range, structural order at $T_{c3} \approx 137$ K. At T_{c3}, the symmetry is lowered to *P*1 with significant changes in the cell parameters. Rb^+ and Cs^+ substitutions that block the N1 and N2 sites selectively show that T_{c1} is related to the torsional motion of the N1 site, while T_{c2} and T_{c3} are governed by the motional slowing down of the N2 site. These data show that the multiferroic behavior of this family is governed by the rotational and translational dynamics of the NH_4^+ ions and is tunable by their controlled substitutions. Relevance to other classes of possible multiferroics is pointed out.

1. INTRODUCTION

Inorganic complexes of Cr in its pentavalent oxidation state (Cr^{5+}) are rather rare.[1] An exception is the class of alkali metal peroxychromates, $M_3Cr(O_2)_4$, M = Li, Na, K, Rb, and Cs, that were first reported by Riesenfeld in 1905,[2] and after several decades investigated for their magnetic dimensionality and phase transitions.[3−6] Recently, we briefly reported that substitution of NH_4^+ in place of alkali metals induces ferroelectric behavior, and that the ferroelectric transition temperature could be varied by growing mixed peroxychromate crystals of alkali metals and ammonium ions.[7] Together with their antiferromagnetic character, the introduction of ferroelectricity elevates these materials to a new class: multiferroics. This finding was considered significant because multiferroic materials, compounds that exhibit long-range ordering of both magnetic and electric nature, are of high research interest since they offer a fundamentally new avenue for information technology: simultaneous control of coding and decoding by electric and magnetic techniques.[8−12] But the earlier study[7] did not clarify the role of various anionic and cationic moieties in the mechanisms of the reported phase transitions. Some of the important queries were as follows: (a) Is the magnetic anion $[Cr(O_2)_4]^{3-}$ involved in the mechanism of the ferroelectric transition at T_{c1}? (b) Do the N1 and N2 sites play specific roles in the various phase transitions? (c) What is the time scale of the polarization fluctuations as a phase transition approaches? (d) Are there any low-lying translational or torsional modes that could be considered as (effective) soft modes leading to the development of lattice polarization at the ferroelectric transition? Answering these questions required additional measurements with techniques specific to each one, and thereby prompted us to undertake the present work.

Received: July 12, 2012
Published: August 30, 2012

   dx.doi.org/10.1021/ja3065705 | *J. Am. Chem. Soc.* 2012, 134, 15953−15962

With the view of answering the above queries, we have carried out more detailed XRD, variable frequency dielectric response studies, low-frequency Raman scattering, and high-frequency (240 GHz) EPR studies on the parent compound $(NH_4)_3Cr(O_2)_4$, ammonium peroxychromate, hereafter referred to as APC. It is shown that the rotational and translational dynamics of the NH_4^+ ions at the two sites, labeled N1 and N2, do indeed play separate and specific roles in the mechanisms of the various transitions. Dielectric relaxation studies reveal a broad peak at T_{c2} (at ~207 K) related to the slow (10^3–10^6 Hz) fluctuations involving the N2 sites. Raman studies complement the XRD results as they show that a ~350 cm^{-1} torsional mode and a 193 cm^{-1} translational mode undergo anomalous changes below the ferroelectric transition at 250 K (T_{c1}). EPR studies on single crystals oriented in different planes show that the reorientational motion of the central magnetic ion $Cr(O_2)_4^{3-}$ also plays a cooperative role in the ferroelectric transition, in concert with the order–disorder motion of the NH_4^+ sites. XRD and specific heat, C_p, measurements on APC crystals heavily doped with Rb^+ and Cs^+ ions show definitively that the displacive behavior of the N1 site is the origin of the 250 K ferroelectric transition (T_{c1}), while the 137 K phase transition at T_{c3} is governed by the motional freezing of the N2 site. All three transitions depend sensitively on the positioning of the alkali cation in the mixed crystals, suggesting a way to modulate the transitions: incorporate the NH_4^+ lattice by replacing the alkali-metal cations in a controlled manner. These results also suggest possibilities for developing new multiferroic families.

2. EXPERIMENTAL SECTION

Single crystals of $M_{3-x}(NH_4)_xCr(O_2)_4$, (where M = Rb, Cs) were synthesized via modification of the method of Riesenfeld[2] by Cage and Dalal.[3] A 20% H_2O_2 solution was added dropwise into an ice cold basic solution (pH = 12) of CrO_3 without stirring over the course of 2–3 h until the solution turned deep red in color. The reaction mixture was then kept at 5–10 °C in a refrigerator for 6–7 days. This procedure of slow cooling and mild evaporation yielded 1 to 2 mm-size tetragonal-looking crystals. XRD studies confirmed the tetragonal structure[3] (vide infra) with the unique (c) axis along the longest dimension. The same procedure was used for synthesizing mixed compounds $M_{3-x}(NH_4)_xCr(O_2)_4$ by using appropriate molar concentrations of MOH and NH_4OH bases.

X-ray structural characterization was done on a Bruker SMART APEX II system using molybdenum radiation. The temperature was controlled by a Kryo-Flex unit. The sample was mounted on a nylon loop. Full data were taken at 263, 203, and 123 K, although other quick scans were carried out at some intermediate temperatures when some confirmation was needed. The reflections were typically indexed using the CELL-NOW programs contained with the SHELXTL suite. As the temperature was lowered below the first phase transition at T_{c1} (250 K), the number of reflections seen in a typical frame increased. They often became less sharp but on returning to a temperature above the upper phase transition, the $I\bar{4}2m$ pattern returned, showing the reversibility of the solid–solid phase transition(s). We did not observe any sign of crystal splitting during the phase changes. Cooling was typically done moderately slowly, over about 3 h. Temperature accuracy was within 2–3°.

A Quantum Design Physical Properties Measurement System (QD PPMS) was used for heat capacity (C_p) measurements over 100–300 K, with a temperature rise of 0.5% employing the usual time constant method.[3−5] Since the mass of one crystal was found to be insufficient, the final sample consisted of 10–15 crystals with a total mass of 2–3 mg in silicon grease. Contribution from the sample platform and silicon grease (addenda) was measured prior to using the sample and subsequently subtracted out. Measurements were also made in magnetic fields up to 9 T, but no significant magnetic field effect was observed, showing little magnetostriction behavior. No significant hysteresis was seen in the position of the C_p peaks on temperature cycling. Temperature accuracy was within 0.1 K.

For dielectric constant measurements, capacitor-type electrodes were made with silver paint on a pair of parallel surfaces of a single crystal. The electrode area was typically 0.2 mm^2, with 0.15-mm separation between the electrodes. A General Radio capacitance bridge was used with frequencies between 400 Hz and 20 kHz. Temperature accuracy was within 0.1 K.

Raman spectra were obtained using a microRaman spectrograph, the JY Horiba LabRam HR800, to allow excitation at 785 nm. Near-infrared spectra were obtained at 785 nm using a TUIOptics (now TOptica Photonics) DL 100 grating-stabilized diode laser emitting 80 mW of power at 785 nm. All lasers were linearly polarized. The spectrograph used a holographic notch filter (785 nm) to couple the laser beam into a microscope (Olympus BX30) by total reflection. The beam was focused on the sample through a microscope objective, which also collected the scattered radiation. The objective chosen depended on the desired focal length and power density on the sample with 5×, 40×, and 50× objectives used to achieve the desired conditions. The notch or edge filter rejected the scattered laser radiation and the Raman scatter was coupled into the spectrograph through a confocal hole. The 800 mm focal length spectrograph used a grating to disperse the Raman scatter onto an 1024×256 element open electrode CCD detector (Wright) which was thermoelectrically cooled to −70 °C to reduce dark noise. The grating selected—either 600 1800 lines/mm—depended on the excitation wavelength, spectral window, and spectral resolution. Since the peroxychromates were sensitive to photo conversion, conditions were chosen to maximize the Raman scatter signal while remaining below the photo conversion threshold. Samples were placed in a Linkam THMS 600 stage allowing temperature studies from 80 K to ambient using liquid nitrogen to cool the stage and provide dry nitrogen purging. Temperature accuracy was within 1–2 K.

High-frequency (240 GHz) EPR spectra were recorded on a locally developed superheterodyne quasi-optical EPR spectrometer available at the National High Magnetic Field Laboratory (NHMFL) in Tallahassee, FL, as described earlier.[13] The spectrometer employs Schottky diode mixer/detectors and a scanable superconducting magnet (Oxford Instruments) capable of reaching 12.5 T. Angular variation was achieved using a goniometer with about 2° precision. Temperature variation was accomplished by using an Oxford continuous helium flow cryostat, over the range of 1.3–400 K with a precision of 0.1 K.

3. RESULTS

3.1. Heat Capacity. While some of the heat capacity, C_p, data were summarized in our preliminary report,[7] we provide here a more detailed discussion for the sake of self-consistency and completeness. Figure 1 shows the data for APC in the

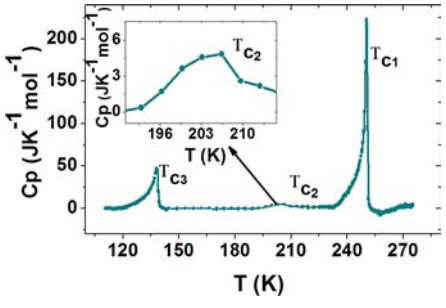

Figure 1. Temperature dependence of excess heat capacity of APC after background removal. Three phase transitions are noted: at T_{c1}= 250 K, T_{c2} = 207 K, and T_{c3} = 137 K. The inset shows the broader peak at 207 K which was not highlighted or discussed in ref 7.

dx.doi.org/10.1021/ja3065705 | J. Am. Chem. Soc. 2012, 134, 15953–15962

100−300 K range. In order to separate the anomalous part related to the phase transitions, a smooth curve was drawn using a baseline method and subtracted from the measured values. This excess specific heat is shown in Figure 1. It is apparent that APC undergoes three phase transitions at temperatures T_{c1} = 250 K, T_{c2} = 207 K, and T_{c3} = 137 K.

The anomalies at 137 and 250 K are sharp and λ-shaped, which is expected for an order−disorder solid−solid phase transition, such as seen for NH_4Cl.[14] However, the peak around T_{c2} = 207 K, as highlighted in the inset of Figure 1, was broader and relatively smaller. In fact, this peak was thought to be part of the background in our earlier studies[7] and was not discussed. The present study shows that this peak is of dynamic origin, with no long-range ordering, since no structural change was seen in the X-ray data, a similar peak was seen in the ac dielectric relaxation measurements (vide infra). The entropy change with this anomaly was found to be rather small, 0.4 J mol^{-1} K^{-1}, in comparison to what is expected for a complete two-site order−disorder phase transition ($R \ln 2$ = 5.76 J mol^{-1} K^{-1}). On the basis of these considerations, this peak is ascribed to some sort of pretransitional short-range ordering related to dynamic slowing down of the N2 site. This short-range ordering culminates in the long-range order that sets in at T_{c3}. Even so, a large part of the residual entropy is removed well below T_{c3} (vide infra), a good sign of relaxor behavior.[14]

3.2. Single-Crystal X-ray Diffraction Studies. In our earlier report,[7] we presented detailed powder XRD data showing the changes in the lattice constants at all of the phase transitions. In this work, we present single-crystal data on APC as well as its mixed crystals (containing Rb^+ and Cs^+ cations substituting for the NH_4^+ ions). XRD data were collected with the crystal well equilibrated into all three phases: for phase I at 263 K, for phase II at 203 K, and for phase III at 123 K, using the same crystal.

3.2.1. Phase I. The basic structure of the room-temperature phase (I) of APC is similar to that of the alkali metal peroxymetallate compounds[4] and could be readily refined in the $I\bar{4}2m$ space group with an R value of 2.47%. As shown in Figure 2, the structure consists of two crystallographically independent NH_4^+ groups (labeled N1 and N2) and a $[Cr(O_2)_4]^{3-}$ unit. N1 is located at a $\bar{4}$ symmetry center and has the usual tetrahedral configuration. N2, on the other hand, is centered at $\bar{4}2m$, exhibiting an orientationally disordered and thus *seemingly* octahedral geometry, not uncommon in the ammonium salts.[15,16] There is a considerable difference between the two types of ammonium nitrogen atoms. The tetrahedral N1 occupies eight positions, two each on the four faces (*ac* and *bc* plane). The nitrogen center N1 is 2.811 Å from 12 oxygen atoms. N2 (along *c* axis) occupies more space and is 2.964−3.012 Å from 8 different oxygen atoms. These differences are important for understanding the bonding and geometry of the mixed crystals grown with Rb^+ and Cs^+ cations substituting NH_4^+, because of the metal ions' very different sizes (vide infra). It should be noted that XRD data showed that the octahedral geometry becomes tetrahedral on cooling to phase III, when the torsional motion of N2 freezes (vide infra).

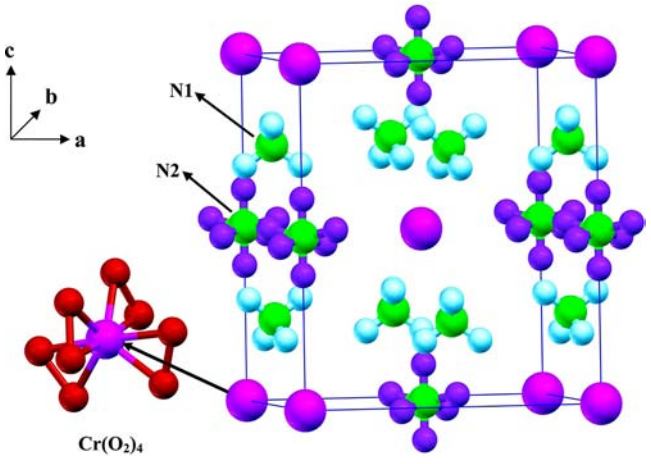

Figure 2. Room-temperature structure of $(NH_4)_3Cr(O_2)_4$. Note that N1 has tetrahedral site symmetry but N2 is orientationally disordered giving rise to *seemingly* octahedral site symmetry. The peroxychromate $(Cr(O_2)_4)^{3-}$ groups are at each corner and center of the unit cell.

3.2.2. Phase II. As the temperature was lowered below 250 K, the reflection pattern changed. At 203 K, the best space group found was $Cmc2_1$. In this space group, the asymmetric unit is $Cr(O_2)_4$ and two of the three N atoms of the NH_4^+ ions and most of the expected hydrogen atoms. The volume of the unit cell was twice that of phase I. Examination of the N−H···O bond distances in phase II showed that the NH_4^+ ions engage in extensive N−H···O hydrogen bonding with essentially all of the peroxo-oxygens of the $Cr(O_2)_4$ moieties.

3.2.3. Phase III. As the temperature was lowered further, below T_{c3} (137 K) to 123 K, the structure was solved in the $P1$ space group. This was done with the large unit cell as a non-merohedral twin using SHELXTL and TWINABS. The twisting of the $Cr(O_2)_4$ groups increased by several degrees. Further, the various atoms become displaced from the ideal edge and face positions of the $I\bar{4}2m$ symmetry as the temperature was lowered from the intermediate phase (phase II) at T_{c2} (~207 K) to phase III below 137 K. The unit cell volume increased slightly from 785.55 to 803.422 Å^3.

Summarizing, at T_{c1}, the ferroelectric transition, the crystal structure changes from tetragonal (phase I) to orthorhombic (phase II). The unit cell volumes doubles with a change in space group from $I\bar{4}2m$ to $Cmc2_1$. No symmetry change was found at T_{c2}, but dynamic studies observed anomalies at T_{c2}, showing that this peak must be associated with a short-range ordering process. Indeed, lattice parameters did show changes as the temperature was lowered below T_{c2}, and these changes leveled off at T_{c3} (137 K). Below T_{c3}, in phase III, the space group changes from $Cmc2_1$ to $P1$. These solid−solid phase changes are all fully reversible with temperature cycling. These conclusions are summarized in Table 1.

Table 1. Crystallographic Data for $(NH_4)_3Cr(O_2)_4$ in Its Three Phases

	263 K, phase I	203 K, phase II	123 K, phase III
a (Å)	6.9951(12)	9.8893(12)	10.00(2)
b (Å)	6.9951(12)	9.889(10)	10.0176(10)
c (Å)	8.028(3)	8.0326(10)	8.0201(10)
α (deg)	90.00	90.00	90.0130(10)
β (deg)	90.00	90.00	90.008(3)
γ (deg)	90.00	90.00	90.004(2)
crystal system	tetragonal	orthorhombic	triclinic
space group	$I\bar{4}2m$	$Cmc2_1$	$P1$
V (Å^3)	392.821	785.55	803.422
R-factor (%)	2.47	2.91	5.67

dx.doi.org/10.1021/ja3065705 | J. Am. Chem. Soc. 2012, 134, 15953−15962

3.3. Dielectric Studies. The overall temperature dependence of the real (ε') and imaginary (ε'') parts of the dielectric constant is shown in Figures 3 and 4, respectively. On

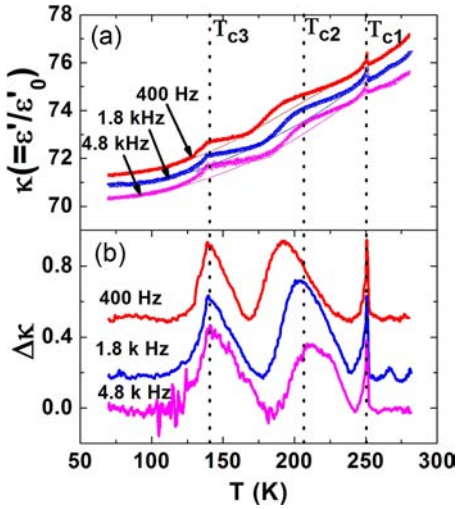

Figure 3. (a) Temperature dependence of the real part of the dielectric constant of APC at selected frequencies. (b) Dielectric constant changes on background subtraction. The data are offset incrementally by 0.1 unit for clarity.

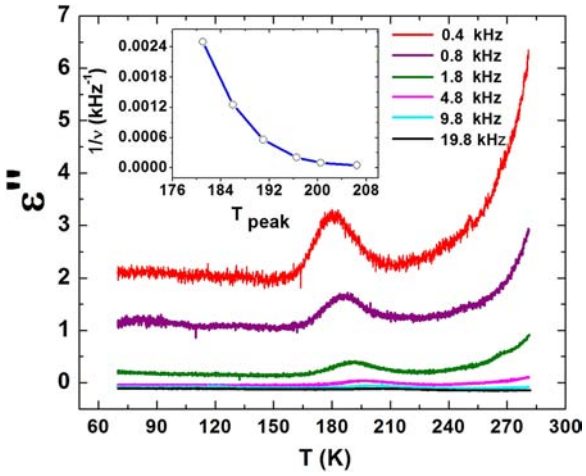

Figure 4. Temperature dependence of the imaginary part of the dielectric constant at selected frequencies. The inset shows frequency dependence of the peak temperatures. The blue line in the inset is a guide to the eye.

temperature lowering below 296 K, in phase I, the real part decreases smoothly, except for an anomalous λ-shaped peak around 250 K, essentially similar to that in the C_p data (Figure 1). A sharp, λ-type anomaly in the real part of the dielectric constant of a material implies a ferroelectric phase transition, although this must be further verified via polarization current or hysteresis-loop measurements.[14] As described in our preliminary report,[7] polarization current data, along with the λ shape of the dielectric peak confirmed that the 250 K phase transition is indeed ferroelectric. Another, broader and smaller peak was seen at about 207 K (T_{c2}), and finally a third one at 137 K (T_{c3}), both in full agreement with the C_p data, Figure 1. It should be noted that the polarization current data showed that neither T_{c2} nor T_{c3} had any noticeable ferroelectric component; they must thus be of a dynamical (T_{c2}) or purely structural nature (T_{c3}). In order to observe the dielectric constant more clearly, the temperature-dependent background was subtracted out and the results for ε' are shown in Figure 3b. The background was obtained by a third order polynomial fitting at different segments assuming smooth increase of the dielectric constant with temperature. It is clear from Figure 3b that the peaks near 250 and 137 K are sharper and not affected by a change in the measurement frequency, consistent with a ferroelectric and a structural transition, respectively. However, the broader peak around 207 K shifts to higher temperatures with increasing frequency. Similar shifts were noted in Figure 4, which shows the temperature and frequency dependence of the imaginary part (dielectric loss). In agreement with the conclusion from Figure 3, only one peak was observed in the dielectric loss (Figure 4), at around 207 K. This peak also shifts to higher temperatures with increasing frequencies, in line with Figure 3. This shift in peak position with frequency shows that the loss is related to a specific molecular motion whose rate of fluctuations coincides with the measurement frequency.[14,15] Overall, the dielectric data strongly support the XRD results in that the ferroelectric transition at 250 K and the structural transition at 137 K are related to the ordering of the N1 and N2 sites, respectively. The 207 K transition must be an orientational mode that slows down to the kHz range, leading to just short-range ordering and formation of pretransitional clusters.

The frequency dependent T_{peak} (Figure 4) was examined for an Arrhenius type behavior,

$$\nu = \nu_0 \exp(-E^a/kT)$$

where E^a is the activation energy barrier between two thermodynamically equivalent sites for ammonium reorientational motion. Figure 5a,b shows plots of ln $(1/\nu(T))$ versus $1/T_{peak}$ for real and imaginary part of the dielectric constant, respectively, where the open circles are experimental data from Figures 3 and 4. The plots and the fits can be seen to be quite linear. We note that real and imaginary part yielded essentially similar activation energies: $E^a_{real} \approx 6500$ K and $E^a_{imag.} \approx 6000$ K. These activation energies are comparable to similar molecules with reorientational disorder.[16]

Figure 6 shows a Cole−Cole plot from the data in Figures 3 and 4. Unfortunately, our available equipment did not provide the frequency range needed for the full Cole−Cole plot. Nevertheless, it can be seen that the data do not yield a semicircle; implicating clearly that there is a distribution of dielectric relaxation times in the ferroelectric phase. This fairly definitive conclusion suggests that the material exhibits the defining characteristics of a relaxor system, in turn opening up an interesting avenue for further studies in this class of multiferroics.

3.4. Raman Studies. Raman studies of low-frequency (100−500 cm^{-1}) modes were undertaken to complement the X-ray studies on the high-frequency side and the dielectric studies at very low frequencies (kHz−MHz), because ferroelectric transitions are known to involve soft modes in this frequency range that show anomalous changes around transition temperatures.[14] Our task was easy because vibrational spectra of tetraperoxometallate compounds with respect to the internal vibrations of the peroxo group in the dodecahedral $[M(O_2)_4]^{3-}$ ion (where M = Cr^{5+}) had been reported before.[17] In particular, it was of interest to study the temperature dependence of the low-frequency rotational, and librational modes of the NH_4^+ ions which lie in this frequency range.[18,19]

dx.doi.org/10.1021/ja3065705 | J. Am. Chem. Soc. 2012, 134, 15953−15962

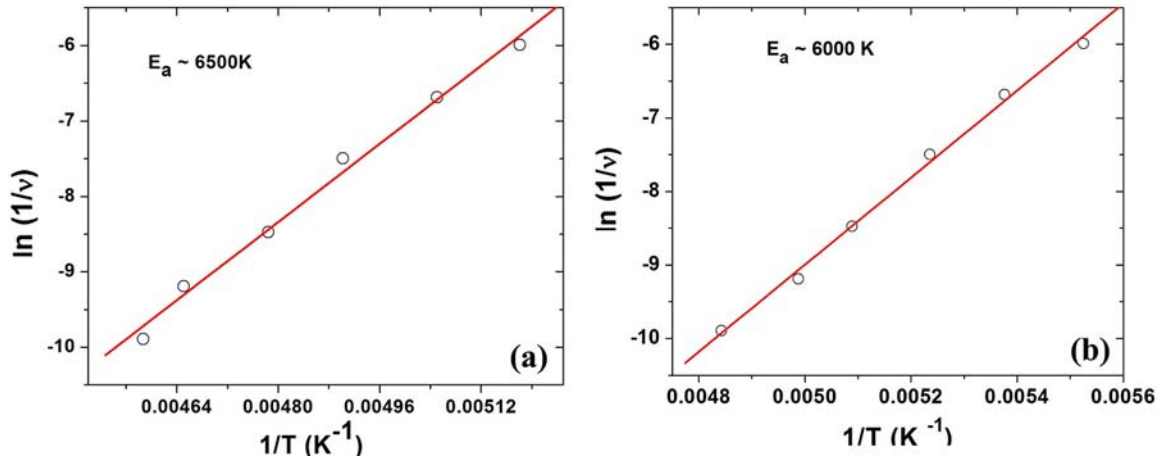

Figure 5. Arrhenius plot of the (a) ε' and (b) ε'' for APC, showing essentially similar activation energies.

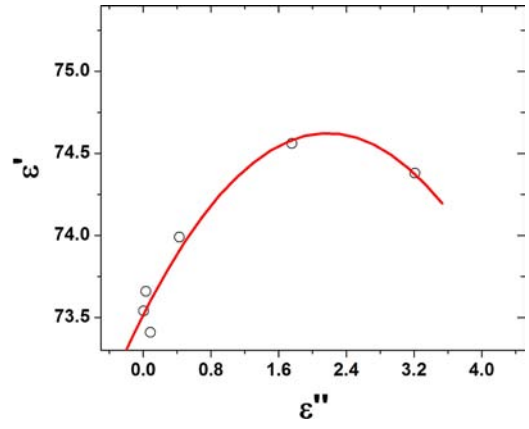

Figure 6. A Cole–Cole plot for APC, indicating multiple relaxation times and hence relaxor behavior in the ferroelectric phase.

Figure 7 shows the temperature dependence of the low frequency Raman spectra. The external optical modes, which are described as rotatory or librational (ν_L) and translational (ν_T) lattice modes of the ammonium group are expected in the 150–400 cm^{-1} range.[20,21] More precisely, the translational modes, υ_T, are expected in the frequency region of 150–250 cm^{-1},[20] and the librational modes in the 300–400 cm^{-1} region.[21] We observed the translational mode at 193 cm^{-1}, that moved significantly (by 13 cm^{-1}) to higher wave numbers on temperature lowering below T_{c1}. The O–Cr–O bending mode appears at 340 cm^{-1} as a broad peak at room temperature. As the temperature was lowered below the orientational order–disorder transition temperature, 207 K, two new peaks appeared which could be assigned to the librational modes representing the C_3 and C_2 rotational motions of NH_4^+ groups.[22,23]

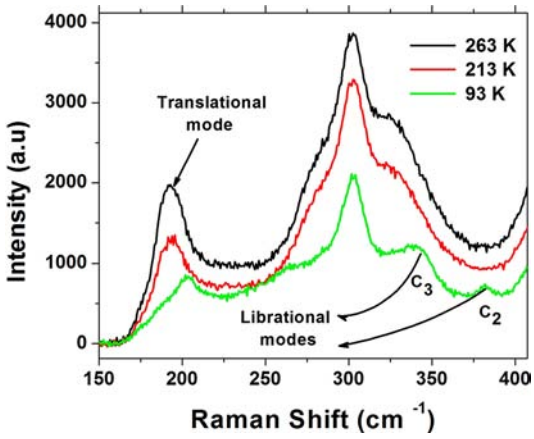

Figure 7. Low frequency Raman spectra of APC at selected temperatures. Note that on temperature lowering, the translational mode around 200 cm^{-1} shifts to higher wavenumbers. The new peaks (342 and 382 cm^{-1}) are attributed to C3 and C2 librational modes, respectively (see text for details).

3.5. High-Frequency EPR. Since this study focuses on multiferroeics, an important goal was to probe the role of the magnetic ion $[Cr(O_2)_4]^{3-}$ in the mechanism of the ferroelectric transition at T_{c1} (250 K). EPR spectroscopy being the most direct technique for probing the structure and dynamics of paramagnetic ions, we initiated EPR studies. We first tried measurements on APC at the low frequency of 9.5 GHz (X-band). The single EPR peak broadened slightly on lowering the temperature through T_{c1}, indicating that the $[Cr(O_2)_4]^{3-}$ moiety must be involved in the phase transition, but the spectral resolution was insufficient to probe the transition mechanism. Higher frequency EPR was then initiated.

Figure 8 shows typical 240 GHz EPR spectra of a single crystal with the orientation of the external magnetic field (H) in the ac plane at the indicated temperatures. A typical Cr^{5+} spectrum is a single peak, involving the $M_S = -^1/_2 \rightarrow {}^1/_2$, $\Delta M_I = 0$ spectroscopic transition at room temperature, as seen here. The spectra could be fully interpreted by the simple spin Hamiltonian containing only the electron Zeeman tensor, as has been demonstrated for other peroxychromates[4–6] but on approaching T_{c1}, at exactly 250 K, the peak split into a doublet, designated as I and II in Figure 8a. It is apparent that the two new peaks represent inequivalent Cr^{5+} centers in the crystal and can be considered as two- sublattices.[24,25] The change in the g-values in both their magnitude and direction (an in-plane rotation by about 10°) clearly shows that at the phase transition, the $[Cr(O_2)_4]^{3-}$ moieties distort and give rise to these two crystallographically inequivalent Cr sites. The very likely reason for the distortion is the hydrogen bonding between the peroxo oxygens and the ammonium group in the APC lattices, which was clearly seen in the crystallographic data (section 3). The EPR-determined phase transition temperature of 250 K (T_{c1}), is in excellent agreement with the above-discussed crystallographic and thermodynamic measurements.

dx.doi.org/10.1021/ja3065705 | J. Am. Chem. Soc. 2012, 134, 15953–15962

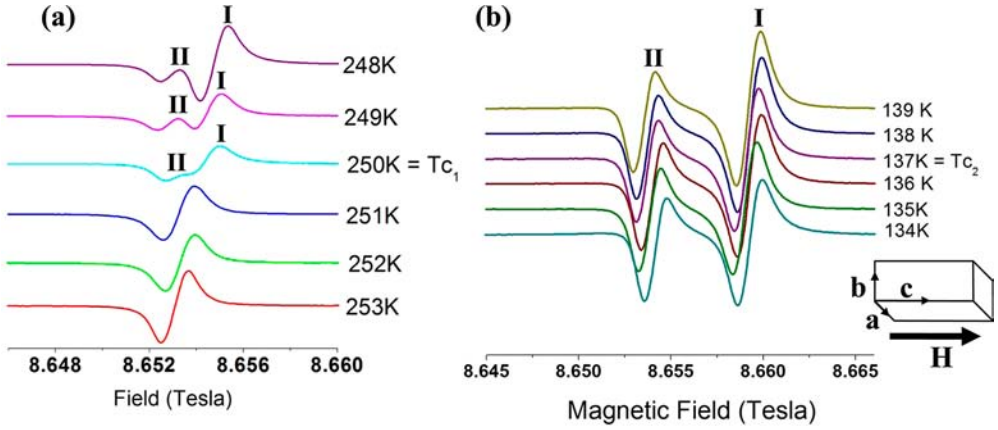

Figure 8. 240 GHz EPR spectra of APC through (a) ferroelectric transition (T_{c1}) and (b) structural transition at 137 K, T_{c3}. The signal splits into two at 250 K (T_{c1}), and some minor changes were observed at 137 K (T_{c3}) (see text).

Figure 9 exhibits the variation of the g value for the orientation of the external magnetic field H in the ac plane, in

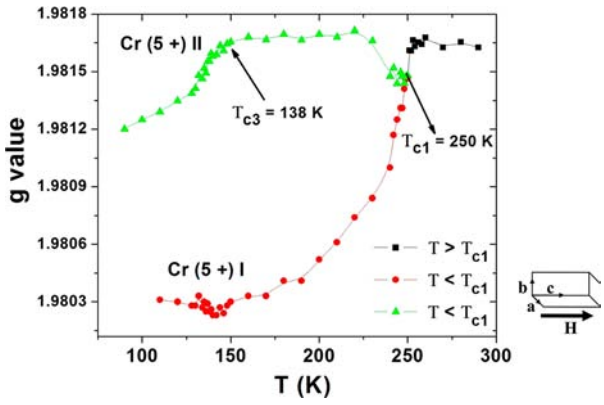

Figure 9. Temperature dependence of g-value of APC at a static magnetic field parallel to c axis. The peak splits at 250 K (T_{c1}) but a decrease in g-value for peak 2 and a small kink for peak 1 are also observed at 137 K (T_{c3}).

the temperature range 30−298 K. As the temperature is decreased, the single peak splits into two at T_{c1} (250 K), supporting the first-order character of this transition at T_{c1}. Below T_{c1}, the g-value corresponding to Cr center II remains constant down to T_{c3} after a small rise but for center I, it undergoes a continuous decrease. Below T_{c3}, the g-value corresponding to Cr center II decreases, whereas that for Cr center I remains nearly invariant. Nevertheless, it is clearly seen that the magnetic moiety $[Cr(O_2)_4]^{3-}$ participates in T_{c1} as well as T_{c3}, clearly due to the strong influence of the N−H···O hydrogen bonding.

The extent of $Cr(O_2)_4$ reorientation at T_{c1} can be seen through the peak splitting pattern, as shown in Figure 10, which shows the angular variation of the g-values for the orientation of magnetic field (H) in the ac plane at above and below the transition at T_{c1}. The crystal was rotated from the c-axis to the a-axis. The signals corresponding to the two magnetically inequivalent Cr(5+) centers (I and II) are quite distinct in the whole plane except at symmetry orientations. The experimental g-value was fitted to the equation $g_{eff}^2 = (g_\perp^2 \sin^2 \theta + g_\parallel^2 \cos^2 \theta)$, and listed in Table 2. Below T_{c1}, $g_\parallel$ =1.9454 and $g_\perp$ = 1.9817 are the same as at room temperature but undergo a rotation of about 10° from the c-axis toward the a-axis. This result clearly

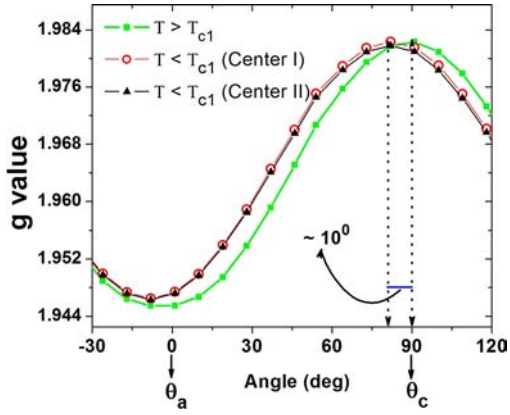

Figure 10. Angular variation of g values obtained from 240 GHz EPR spectra of APC above and below T_{c1}= 250 K) for the magnetic field in the ac plane. θ_a and θ_c represent the a and c axis, respectively. Note that the g maxima or minima are shifted by 10° below T_{c1} (shown by the arrow), showing the rotation of the $Cr(O_2)_4$ dodecahedra accompanying the ferroelectric transition. The curves are fits with $g_{eff}^2 = g_\perp^2 \sin^2 \theta + g_\parallel^2 \cos^2 \theta$.

Table 2. g Values of APC below and above T_{c1}

temp, Cr^{5+} site	$g_\perp$	$g_\parallel$
260 K ($T > T_{c1}$)	1.9817	1.9454
240 K, Cr^{5+} I ($T < T_{c1}$)	1.9818	1.9468
240 K, Cr^{5+} II ($T < T_{c1}$)	1.9815	1.9462

shows that the paramagnetic $[Cr(O_2)_4]^{3-}$ center twists by ~10° due to the ferroelectric transition at T_{c1}, in conformity with the single-crystal XRD studies [see Supporting Information, Figure S1].

3.6. Mixed $M_x(NH_4)_{3-x}Cr(O_2)_4$ (M = Rb, Cs) Crystals Elucidate the Specific Role of the N1 and N2 Sites. As mentioned in the Introduction, an important part of this study was to elucidate the specific role of the N1 and N2 sites in the three phase transitions in APC and to find a chemical procedure to control the transition temperatures. One way was to block the role of say the N1 and N2 sites in a specific ratio and examine the transition behavior, and this is the strategy that was undertaken. Since the size of Rb^+ is essentially the same as that of NH_4^+ (Rb^+ = 1.49 Å and NH_4^+ = 1.43 Å),[26,27] Rb^+ should thus substitute the larger N2 sites easily but also N1 sites. However, since Cs^+ is significantly larger than

dx.doi.org/10.1021/ja3065705 | J. Am. Chem. Soc. 2012, 134, 15953−15962

NH_4^+ (Cs^+ = 1.65 Å, NH_4^+ = 1.43 Å),[27,28] Cs^+ should substitute only the N2 site exclusively. We thus grew these mixed crystals and, as discussed below, our expectations did indeed pan out.

3.6.1. Crystal Structure of $Rb_{1.36}(NH_4)_{1.64}Cr(O_2)_4$. Crystal structure of the mixed Rb–ammonium peroxychromate (RAPC) was solved at room temperature with an *R* value of 2.42%. In a typical preparation, the composition was found as $Rb_{1.36}(NH_4)_{1.64}Cr(O_2)_4$. The structure is isomorphic with that of APC, tetragonal, space group $I\bar{4}2m$. The structure is shown in Figure 11. The Rb ion is found exclusively in the N2 site and

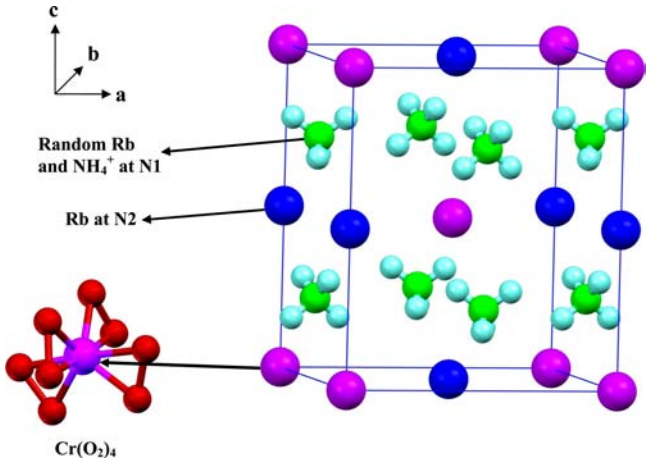

Figure 11. Room-temperature structure of RAPC showing Rb substituting the larger N2 site. The site N1 is shared randomly by Rb and NH_4 ions. $[Cr(O_2)_4]^{3-}$ groups are at each corner and center of the unit cell.

N1 is occupied by a mixture of the two ions. The overall formula can be thought of as $(Rb_{1.00})(Rb_{0.36})(NH_4)_{1.64}Cr(O_2)_4$. Thus, $Rb_{1.00}$ effectively blocks the N2 site. Table 3 summarizes the structural data (vide infra).

Table 3. Room-Temperature Crystal Structure Data on the Mixed Crystals RAPC and CAPC

chemical formula	$Rb_{1.34}(NH_4)_{1.64}Cr(O_2)_4$	$Cs(NH_4)_2Cr(O_2)_4$
temp (K)	267	263
a (Å)	6.9862(3)	7.0386(3)
b (Å)	6.9862(3)	7.0386(3)
c (Å)	7.9044(6)	8.1748(8)
α (deg)	90.00	90.00
β (deg)	90.00	90.00
γ (deg)	90.00	90.00
crystal system	tetragonal	tetragonal
space group	$I\bar{4}2m$	$I\bar{4}2m$
V (Å^3)	385.79	404.995
R-factor (%)	2.42	1.22

3.6.2. $Cs(NH_4)_2Cr(O_2)_4$ (CAPC). Single-crystal X-ray measurements at room temperature showed that $Cs(NH_4)_2Cr(O_2)_4$ (hereafter CAPC) is also isomorphic with APC, with the tetragonal space group $I\bar{4}2m$ (*R* value of 1.22%). The Cs^+ ion clearly occupies exclusively the (larger) N2 site, because of its larger size as compared to that of the NH_4^+ ions. The NH_4^+ ions occupy the N1 sites with double occupancy at the four faces. The structure is shown in Figure 12. Table 3 summarizes the crystal structure data on RAPC and CAPC.

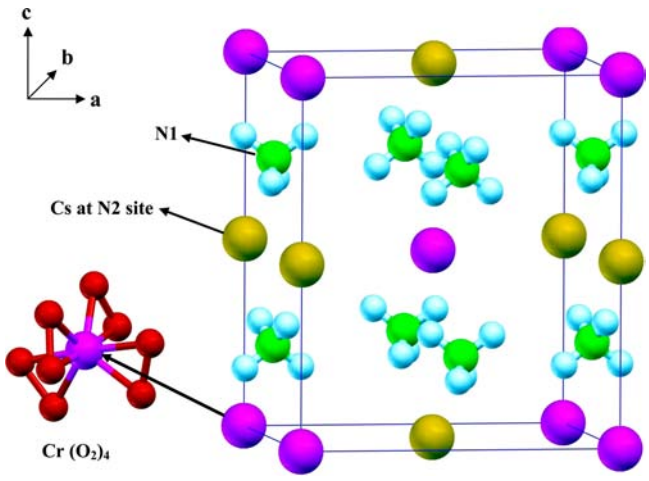

Figure 12. Room-temperature structure of CAPC, showing Cs^+ substituting all the N2 sites exclusively. The $[Cr(O_2)_4]^{3-}$ groups are at each corner and center of the unit cell.

3.6.3. Heat Capacity Studies on Mixed Crystals. Heat capacity measurements were performed on RAPC and CAPC to determine any shift in the T_{c1} and T_{c3} temperatures due to the substitution of the NH_4^+ cations by the Rb^+ and Cs^+ ions. As shown in Figure 13 for RAPC, the changes in the heat

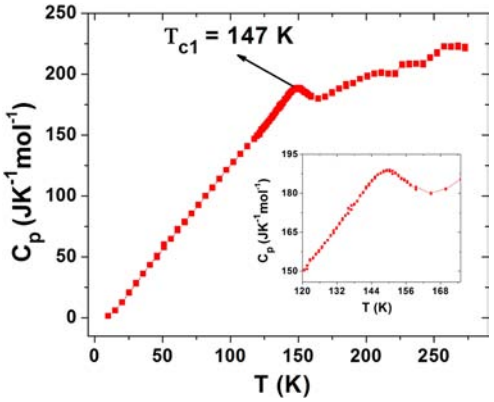

Figure 13. Temperature dependence of heat capacity of RAPC. The inset shows the nature of the peak (broad) at phase transition temperature.

capacity relative to APC were dramatic: T_{c1} moved to the lower temperature of 147 K, while T_{c2} and T_{c3} did not appear at all even down to 1.8 K. The data for CAPC were similar, as shown in Figure 14: T_{c1} moved down to 158 K, while T_{c2} and T_{c3} were not observable down to 1.8 K. The excess specific heats of RAPC and CAPC were obtained after subtraction of the baseline from the heat capacity data by the positive algorithm method of the Origin program. The entropy of the phase transitions of RAPC and CAPC were calculated by integrating the area of the phase transition region: $\Delta S = \int (C_p/T)\, dT$. The entropies were found to be 3.12 and 2.47 J mol^{-1} K^{-1} for RAPC and CAPC, respectively. Although the obtained entropies of the phase transitions deviate from that of an order–disorder phase transition, 5.76 J mol^{-1} K^{-1}, the phase transition may be still classified as of an order–disorder type,[29] since all of the entropy might not have been expended in the transition process, some residual entropy is always left over if the transition has some relaxor character. As discussed below, some

dx.doi.org/10.1021/ja3065705 | J. Am. Chem. Soc. 2012, 134, 15953–15962

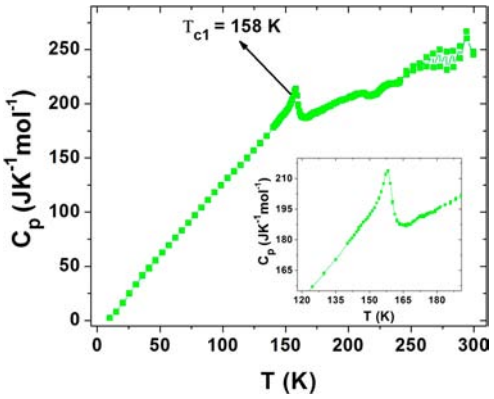

Figure 14. Temperature dependence of heat capacity of CAPC. The inset shows the nature of the peak at phase transition temperature.

evidence for the relaxor behavior is seen in the dielectric relaxation studies.

The heat capacity peak became broader, the broadening increasing from APC to CAPC to RAPC, in inverse proportion to the NH_4^+ ion concentration in the crystal. The sharper heat capacity peak suggests a near first-order phase transition and broader peaks correspond to second order behavior.[30] The shapes of the C_p peaks in RAPC and CAPC can be clearly seen in the insets of Figures 13 and 14. From these results, it may be inferred that the amount of NH_4^+ ion in the crystal controls the nature of phase transitions in this family of crystals. In fact, it was earlier noted[7] that T_{c1} is a linear function of $[NH_4^+]$ content relative to the alkali metal.

How exactly does the relative amount of the NH_4^+ to Cs^+ lead to a near-first order transition in CAPC as compared to second-order transition in RAPC? A clue to this query is provided by the fact that the Cs^+ ion substitutes only at N2 sites at the 4 axis (along *c* axis), a clean lattice, hence the cooperative phase transition process is much like that for the pure NH_4^+ case, except at a lower temperature. However, Rb substitutes in a more random way both along the edges and at the faces (*ac* and *bc* planes) of the tetragonal lattice. Thus there must be a distribution of the locally polarized domains across the RAPC lattice. The phase transition temperature would be expected to have a distribution; hence the C_p peak would be expected to be broader, like for a second-order phase transition.

Summarizing, XRD data show that the mixed compounds CAPC and RAPC have essentially the same crystal symmetry as APC, except that the Cs and Rb ions substitute N1 and N2 sites specifically: Cs replaces the N2 sites specifically whereas Rb goes into both N2 and N1 sites. This result in turn provides direct support for the origin of the transitions at T_{c1} and T_{c3}, as discussed below.

4. DISCUSSION OF THE FERROELECTRIC TRANSITION MECHANISM

4.1. Summary of Single-Crystal Data on APC, RAPC, and CAPC. On the basis of the presented single-crystal XRD data on APC, RAPC, and CAPC, we can propose a model/mechanism for the ferroelectric transition at T_{c1} (250 K). Figure 15 shows an atomistic view of this transition. The two independent NH_4^+ sites N1 and N2 are shown with green and red balls, respectively. It is seen that the N1 sites which exhibit the normal, tetrahedral, geometry at room temperature (phase I) get displaced along the *b* axis at T_{c1}, whereas the orientationally disordered N2 sites stay at their original positions. The unit cell lengths *a* and *b* increase by $\sqrt{2}$ times than in its room-temperature phase to accommodate the displaced ammonium groups in the unit cell and hence the cell

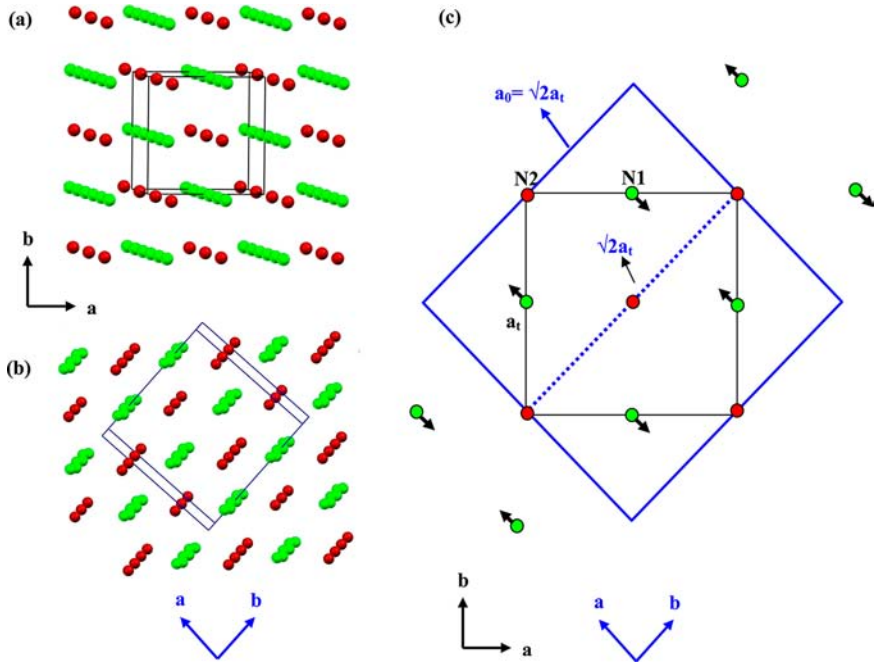

Figure 15. (a) Crystal structure of APC showing only N atoms of NH_4^+ groups along *c* axis at (a) 263 K (tetragonal phase) and (b) 203 K (orthogonal phase). Green balls represent N1 and red balls N2 sites. (c) Model for phase transition mechanism of APC. The black square shows the square face of the tetragonal cell with space group $I\bar{4}2m$ and the blue rectangle shows the orthorhombic unit cell with space group $Cmc2_1$. The small thick black arrows show the direction of displacement of ammonium group N1 during the 250 K ferroelectric phase transition. Note: Only N1 ammonium groups are displaced.

dx.doi.org/10.1021/ja3065705 | J. Am. Chem. Soc. 2012, 134, 15953−15962

volume doubles.[7] Thus the transition at 250 K (T_{c1}) can be seen to be governed by the displacement of the N1 sites, without any significant participation from the N2 sites.

Our Raman data on the translational modes at ~193 cm^{-1} (Figure 16) support this displacement model, as there is an

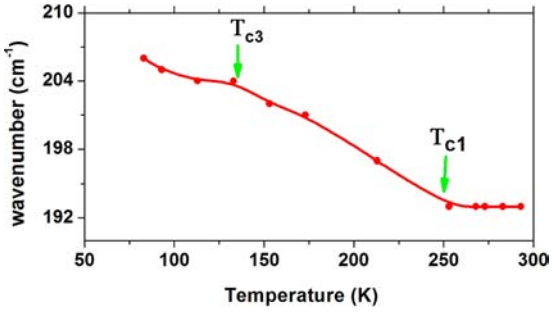

Figure 16. Temperature dependence of 193 cm^{-1} translational mode of NH_4^+ ions in APC. Notice the gradual slope change at T_{c1} and T_{c3}.

anomalous change in this mode on temperature lowering below 250 K. This mode shifts to higher frequencies by about 15 cm^{-1}, starting at T_{c1} going toward T_{c2} and stops changing at T_{c3}. Similarly, the space group change at T_{c3} (137 K) and thus the solid–solid phase transition at this temperature could be ascribed to the motional freezing[31] and distortion around the N2 site.

The C_p data on CAPC strongly support the conclusion that the N2 site is directly involved in the mechanism of T_{c3}. Since CAPC has no NH_4^+ ions at the N2 site, the observed transition T_{c1} in CAPC must arise from the NH_4^+ ions at the N1 site only. The lower temperature of this transition (158 K) than in APC (T_{c1} = 250 K) is in line with the smaller fraction of the NH_4^+ ions in the CAPC lattice. The C_p data on RAPC are consistent with these conclusions. The studies on the mixed compounds were thus useful not only for elucidating the role of the specific ammonium sites in the mechanism of the three transitions in APC, they also indicated a procedure for controlling the ferroelectric transition temperatures (T_{c1}), and T_{c3} in these new multiferroics.

The broad maximum around 207 K in the dielectric relaxation measurements is frequency dependent and seen clearly in the dielectric loss component (Figure 4). As is well-established, such a peak arises when the effective frequency of a certain mode of fluctuations, defined by $1/\tau$ (τ the relaxation time), coincides with that of the applied ac electric field. This dielectric dispersion peak indicates a typical relaxor behavior with the dielectric constant decreasing with increasing frequency and the maximum shifting to higher temperatures.[14] This discovery of the relaxor behavior in this new class of multiferroics opens an exciting new area of further studies on these materials.

5. CONCLUSIONS

This study shows that ferroelectric behavior can be induced in alkali metal peroxychromates, $M_3Cr(O_2)_4$, M = Rb and Cs, by carefully introducing NH_4^+ cations in the lattice. If the salts are magnetic, then the materials could exhibit multiferroic character, which is of high current research interest with regard to memory storage and manipulation in a novel way: using electric and magnetic controls, simultaneously. We have provided detailed X-ray crystallographic, thermodynamic, dielectric relaxation, EPR, and Raman spectroscopic evidence for the atomistic details of the mechanism underlying the ferroelectric and related transitions: the motional degrees of freedom of the NH_4^+ ions.[31] It is shown that the transition temperature and its sharpness can be tuned by careful cation substitutions. In the mixed lattices, the ferroelectric character seems to be of a relaxor type, a potentially new area of research in the multiferroic families. It occurred to us also that similar procedures can be used to induce ferroelectricty in paramagnetic compounds of other ions, such as the $MCuCl_3$ family, with M = K, Rb, Cs, Tl. We have initiated research in this area, and the results seem quite promising.[32] Finally, we note that it is important to understand the electronic mechanisms of multiferroic behavior, along the lines suggested in several recent papers,[8,33−35] and references contained therein.

■ ASSOCIATED CONTENT

Ⓢ Supporting Information

Crystallographic data (CIF) and the structure showing the twisting of $Cr(O_2)_4$ moiety by ~10° below the ferroelectric phase transition. This material is available free of charge via the Internet at http://pubs.acs.org.

■ AUTHOR INFORMATION

Corresponding Author

dalal@chem.fsu.edu

Notes

The authors declare no competing financial interest.

■ ACKNOWLEDGMENTS

We thank Dr. Bert Van de Burgt for help with the Raman measurements. HF-EPR, and dielectric measurements were carried out at NHMFL, Tallahassee, FL. We are grateful to Drs. Z. Wang and J. van Tol for help with the EPR measurements. NHMFL is supported by the NSF Cooperative agreement DMR 0654118, the State of Florida, and DOE.

■ REFERENCES

(1) (a) Dickman, M. H.; Pope, M. T. *Chem. Rev.* **1994**, *94*, 569. (b) Cotton, F. A.; Wilkinson, G.; Murillo, C. A.; Bochmann, M. *Advanced Inorganic Chemistry*, 6th ed.; John Wiley and Sons; Inc.: New York, 1999; p 749.

(2) Riesenfeld, E. H. *Chem. Ber.* **1905**, *38*, 4068.

(3) Cage, B.; Geyer, W.; Abboud, K. A.; Dalal, N. S. *Chem. Mater.* **2001**, *13*, 871.

(4) Cage, B.; Dalal, N. S. *Chem. Mater.* **2001**, *13*, 880.

(5) Ramsey, C. M.; Cage, B.; Abboud, K. A.; Dalal, N. S. *Chem. Mater.* **2003**, *15*, 92.

(6) (a) Choi, K.-Y.; Nellutla, S.; Reyes, A. P.; Kuhns, P. L.; Jo, Y.-J.; Balicas, L.; Nojiri, H.; Pati, M.; Dalal, N. S. *Phys. Rev. B* **2008**, *78*, 214419. (b) Nellutla, S.; Pati, M.; Jo, Y.-J.; Zhou, H. D.; Moon, B. H.; Pajerowski, D. M.; Yoshida, Y.; Janik, J. A.; Balicas, L; Lee, Y.; Miesel, M. W.; Takano, Y.; Wiebe, C. R.; Dalal, N. S. *Phys. Rev. B* **2010**, *81*, 064431.

(7) Samantaray, R.; Clark, R. J.; Choi, E. S.; Zhou, H.; Dalal, N. S. *J. Am. Chem. Soc.* **2011**, *133*, 3792.

(8) Spalding, N. A.; Cheong, S.; Ramesh, R. *Phys. Today* **2010**, *63* (10), 38. (b) Cheetham, A. K.; Rao, C. N. R. *Science* **2007**, *318*, 58.

(9) Ghosez, P.; Triscone, J.-M. *Nat. Mater.* **2011**, *10*, 269.

(10) Lebeugle, D.; Colson, D.; Forget, A.; Viret, M.; Bataille, A. M.; Gukasov, A. *Phys. Rev. Lett.* **2008**, *100*, 227602.

(11) Rovillain, P.; de Sousa, R.; Gallais, Y.; Sacuto, A.; Méasson, M. A.; Colson, D.; Forget, A.; Bibes, M.; Barthélémy, A.; Cazayous, M. *Nat. Mater.* **2010**, *9*, 975.

(12) (a) Jain, P.; Dalal, N. S.; Toby, B. H.; Kroto, H. W.; Cheetham, A. K. *J. Am. Chem. Soc.* **2008**, *130*, 10450. (b) Jain, P.; Ramachandran,

V.; Clark, R. J.; Zhou, H. D.; Toby, B. H.; Dalal, N. S.; Kroto, H. W.; Cheetham, A. K. *J. Am. Chem. Soc.* . **2009**, *131*, 13625.
(13) Van Tol, J.; Brunel, L. C.; Wylde, R. J. *Rev. Sci. Instrum.* **2005**, *76*, 074101.
(14) Lines, M. E.; Glass, A. M. *Principles and Applications of Ferroelectrics and Related Materials*; Oxford University Press: New York, 1977.
(15) Chen, R. H.; Yen, C.-C.; Shern, C. S.; Fukami, T. *J. Appl. Phys.* **2005**, *98*, 044104.
(16) Shin, H. K. *Solid State Commun.* **2003**, *128*, 131.
(17) Haeuseler, H.; Haxhillazi, G. *J. Raman Spectrosc.* **2003**, *34*, 339.
(18) Shurvell, H. F.; Brown, R. J. C.; Korppi-Tommola, J. *J. Raman Spectrosc.* **1980**, *9*, 28.
(19) Rubin, J.; Bartolom, J.; Laguna, M. A.; Sanjufin, M. L. *Physica B.* **1996**, *217*, 227, also 234.
(20) Laguna, M. A.; Sanjuan, M. L.; Orera, V. M.; Rubin, J.; Palacios, E.; Pique, M. C.; Bartolome, J.; Berar, J. F. *J. Phys. Condens. Mater.* **1993**, *5*, 283.
(21) Korppi-Tommola, J.; Devrajan, V.; Brown, R. J. C.; Shurvell, H. F. *J. Raman Spectrosc.* **1978**, *7*, 96.
(22) Brown, R. J. C.; Alavi, A.; Lynden-Bell, R. M. *J. Chem. Phys.* **1999**, *110*, 5861.
(23) Carter, R. L.; O'Hare, L. K. *Appl. Spectrosc.* **1976**, *30*, 187.
(24) (a) Dalal, N. S.; Millar, J. M.; Jagadeesh, M. S.; Seehra, M. S. *J. Chem. Phys.* **1981**, *74*, 1916. (b) Cage, B.; Hassan, A.; Pardi, L.; Krzystek, J.; Brunel, L. C.; Dalal, N. S. *J . Magn. Reson.* **1997**, *124*, 495.
(25) Misra, S. K.; Sun, J.; Jerzak, S. *Phys. Rev. B* **1989**, *40*, 74.
(26) Marchal-Roch, C.; Laronze, N.; Guillou, N.; Teze, A.; Herve, G. *Appl. Catal., A* **2000**, *203*, 143.
(27) Van Niekerk, J. N.; Schoening, F. R. L. *Acta Crystallogr.* **1952**, *5*, 475.
(28) Clark, M. J. R.; Lynton, H. *Can. J. Chem.* **1969**, *47*, 2579.
(29) Yamamura, Y.; Nakajima, N.; Tsuji, T. *Solid State Commun.* **2000**, *114*, 453.
(30) Hatta, I.; Nakayama, S. *Thermochim. Acta* **1998**, *318*, 21.
(31) Smith, D. *Chem. Rev.* **1994**, *94*, 1567.
(32) Kinyon, J.; Florida State University, personal communication, June 2012.
(33) Lee, J. H.; Fang, L.; Vlahos, E; et al. *Nature (London)* **2010**, *466*, 954.
(34) Ramesh, R; Spaldin, N. A. *Nat. Mater.* **2007**, *6*, 21.
(35) (a) Fennie, C. J.; Rabe, K. M. *Phys. Rev. Lett.* **2006**, *97*, 267602. (b) Lee, I. H.; Rabe, K. M. *Phys. Rev. Lett.* **2010**, *104*, 207204.